

Symmetry un-breaking in the shapes of perfect projectiles.

Marcus Roper,¹ Todd M. Squires,² and Michael P. Brenner¹

¹*School of Engineering and Applied Sciences, Harvard University*

²*Department of Chemical Engineering, U.C. Santa Barbara*

(Dated: September 5, 2007)

We study the shapes of perfect projectiles: bodies of prescribed volume that are designed to suffer minimum fluid drag in steady flight. Perfect projectiles have a surprising property: although the flow of fluid around the body of the projectile is fore-aft asymmetric at moderate flow speeds, the shape of the body that minimizes drag is nonetheless highly symmetrical. We show that perfect projectiles are weakly asymmetric and that their asymmetry grows with the cube of the projectile size for sufficiently small projectiles. The persistence of apparent fore-aft symmetry is speculated to be a signature of the linearity and reciprocity of the drag determining features of the flow around the projectile.

PACS numbers: Valid PACS appear here

For locomotion at high speeds, slender shapes with blunt noses and sharp trailing edges are favored for drag reduction, as can be seen in the body forms of fish evolved for high speed cruising like tuna or mackerel, or in the design of modern aerofoils. Drag minimization is not simply a selection pressure upon large, fast moving predators with conspicuously streamlined shapes, but is also significant at the microscale. Fluid drag encountered in flight severely limits the range of explosively launched propagules, such as seeds or fungal spores; Vogel estimates that the ascospores of the “fungal gun” *Giberella zeae* lose 99.997% of their potential range to drag [1].

It is natural to ask whether, and in which respects, bauplans have been influenced by selection pressure to minimize drag while conserving propulsive capacity [2, Chapter 7]. Identification of drag determining features of large rapidly swimming animals has been aided by comparison of animal morphologies and measured drags with the shapes and reported drags of high speed aerofoils or flat plates of matching volume or area. Such comparisons originate with von Kármán who first noted the remarkably precise agreement between the shapes of trout in dorsal-ventral section and the profile of a modern aerofoil [3]. We attempt to extend such comparisons into the realm of moderate Reynolds numbers (i.e. $Re \lesssim 100$) inhabited by the smallest (and most drag-constrained [1]) bioprojectiles, by computing the shapes of *perfect projectiles*: bodies with prescribed volume and speed that are shape so as to suffer minimum fluid drag in steady flight.

Few of the properties of perfect projectiles are known. Questions such as what increase in range or flight speed an organism can attain by redistributing mass to attain a drag-minimizing shape remain unanswered. The penalties of drag minimization also remain poorly quantified: whether minimal-drag shapes are undesirable according to some other criteria, such as poor stability in flight or low stall-angle. Here we make a first step toward a full characterization of the properties of minimal-drag shapes by investigating the variation of fore-aft asymmetry with Reynolds number. We find that although the flow around the body and the pattern of surface stresses

are both highly asymmetric, perfect projectiles remain relatively fore-aft symmetric up to moderate Reynolds numbers. We call this an “unbroken asymmetry”: an instance where an asymmetric action (the fluid drag functional) has a highly symmetric minimum. Asymptotic studies illuminate the slow increase in asymmetry of the minimum from vanishingly small Reynolds numbers. The persistence of symmetry at moderate Reynolds numbers is argued to be a signature of the underlying reciprocity and linearity of the drag determining features of the flow.

I. COMPUTATION OF MINIMUM DRAG SHAPES

We determine numerically the shapes of perfect projectiles for prescribed volumes and flight speed. The joint effect of varying flight speed and body size is represented by a single dimensionless group: the *Reynolds number* $Re = Ua/\nu$, in which U is the speed of flight, and a is a characteristic body dimension (here we identify a with the radius of a sphere of equivalent volume to the projectile). The minimal drag shape has already been determined for slowly creeping flows ($Re = 0$) [4, 5], and an algorithm for determining the minimal drag shape proposed for flows at arbitrary Re [6], but has previously only been implemented for flow around two-dimensional bodies at a limited set of flow speeds [7]. We determine axisymmetric minimal drag body shapes using an algorithm similar to that suggested by Pironneau [6].

The core of our method for determining the shapes of perfect projectiles is a calculation of how an arbitrary infinitesimal deformation to the boundary of a given projectile affects the fluid drag that the projectile would experience in flight. Once known, we may start with an arbitrary initial projectile shape, and then use steepest descent may be used to make successive optimal refinements to the boundary until a drag minimum is achieved.

In order to compute the change in drag upon a projectile, denoted by Ω , immersed in an infinite body of fluid, due to a small perturbation to the boundary of the

shape $\partial\Omega$, we represent the drag upon the projectile by a functional:

$$L[\Omega] = \int_{\partial\Omega} \mathbf{n} \cdot \boldsymbol{\sigma} \cdot \mathbf{U} dS + \int_{\mathbb{R}^3 - \Omega} [\mathbf{w} \cdot (\nabla \cdot \boldsymbol{\sigma} - \rho(\mathbf{u} \cdot \nabla)\mathbf{u}) + q\nabla \cdot \mathbf{u}] dV + \lambda \left(\int_{\Omega} dV - |\Omega| \right), \quad (1)$$

in which the first term denotes the rate of working of the drag force, and the adjoint velocity (\mathbf{w}) and pressure (q) fields that appear in the second term are Lagrange multipliers that we introduce in order to enforce, respectively, the conservation of momentum and incompressibility of the flow. A third Lagrange multiplier λ constrains the volume of the body [8].

Consider a small deformation to the the projectile bounding surface in which each boundary point \mathbf{x} is moved to a point $\mathbf{x} + \alpha(\mathbf{x})\mathbf{n}$, for some function $\alpha(\mathbf{x})$ that remains small over the entire of the boundary. Provided the adjoint fields satisfy an equation

$$-\nabla q + \eta \nabla^2 \mathbf{w} = -\rho(\mathbf{u} \cdot \nabla)\mathbf{w} + \rho(U_j + w_j)\nabla u_j, \quad (2)$$

with $\nabla \cdot \mathbf{w} = 0$, $\mathbf{w} = \mathbf{0}$ on the boundary of the shape and $\mathbf{w} \rightarrow -\mathbf{U}$ in the far-field, the change in the (rate-of-working of the) drag, δL , can be cast in the form of a single integral over the unperturbed surface of the body:

$$\delta L = - \int_{\partial\Omega} \alpha(\mathbf{x}) \left(\eta \frac{\partial \mathbf{u}}{\partial \mathbf{n}} \cdot \frac{\partial \mathbf{w}}{\partial \mathbf{n}} + \lambda \right) dS. \quad (3)$$

We call (2) and the solenoidal condition that follows it the *adjoint* equations. A minimal drag shape must have δL vanishing for all volume-preserving (i.e. having the property that $\int_{\partial\Omega} \alpha dS = 0$) boundary perturbations, and must therefore have $J \equiv \frac{\partial \mathbf{u}}{\partial \mathbf{n}} \cdot \frac{\partial \mathbf{w}}{\partial \mathbf{n}}$ uniform over the entire of the boundary.

We now have means to calculate an optimal deformation to the boundary of the shape [4], chosen to be a perturbation that achieves maximum drag benefit while fixing the volume of the shape:

$$\alpha(\mathbf{x}) \propto \eta \frac{\partial \mathbf{u}}{\partial \mathbf{n}} \cdot \frac{\partial \mathbf{w}}{\partial \mathbf{n}} - \frac{\eta}{|\partial\Omega|} \int_{\partial\Omega} \frac{\partial \mathbf{u}}{\partial \mathbf{n}} \cdot \frac{\partial \mathbf{w}}{\partial \mathbf{n}} dS, \quad (4)$$

where we arrive at the second term by choosing λ to ensure that $\int_{\partial\Omega} \alpha dS = 0$. Now we imagine parameterizing the sequence of shapes that the body must pass through from the initial shape to the minimal drag shape by some parameter μ , and identify $d\mathbf{x}/d\mu$ as $\alpha\mathbf{n}$. Previous implementations of the gradient-descent method for drag minimization have integrated the equation for the sequence of shapes passed through by the body using a fixed step size scheme, and encountered instabilities in the boundary shape, which must then be removed by filtering [7]. We avoid such instabilities by integrating the equation using a low-order variable step-size routine (the Matlab

function `ode23`), and by permitting very small step sizes, at the cost of more, costly, evaluations of the function α . For each of the shapes in the sequence, the coupled Navier-Stokes and adjoint equations (2) are solved using COMSOL Multiphysics, and the optimal boundary perturbation (i.e. $d\mathbf{x}/d\mu$ for each of the vertices on the boundary) subsequently determined. Approach toward the minimal drag shape is tested for by measuring the convergence of the integrand J to a uniform value along the shape-boundary.

II. PRESERVATION OF SYMMETRY UP TO MODERATE REYNOLDS NUMBERS

In figure 1(a) shapes of perfect projectiles are plotted for Reynolds numbers ranging from 0.1 up to 100. This interval in Reynolds number would correspond for a 20 μm long body traveling through air ($\nu = 1.8 \times 10^{-5} \text{ m}^2\text{s}^{-1}$) to flight speeds ranging from 0.1 up to 100 ms^{-1} , which covers the full range of estimated launch conditions of explosively launched fungal propagules [1].

We observe that each of the minimal drag shapes is very fore-aft symmetric: resourceful readers are challenged to guess, without consulting the figure caption, whether projectiles are designed for flight in the positive or in the negative z -direction! A more careful quantification of the slow emergence of asymmetry is given in panel (b) of the figure, in which we chart the growth of projectile asymmetry with $\mathcal{R}e$ via the third moment

$$M_3 = \frac{3 \int_{\Omega} (z - \bar{z})^3 dV}{4\pi L^3}, \quad (5)$$

where L is the total length of the body, and $\bar{z} = 3 \int_{\Omega} z dV / 4\pi$ is the first moment of the projectile. We make this measure of asymmetry more intelligible by plotting, on the same figure, values of M_3 for a reference shape of volume equal to that of our perfect projectile and with controllable asymmetry. We form this shape by compounding two hemispheroids of different major axes l_1, l_2 (and with common minor axis d fixed by the constraint upon the volume of the shape). For such a body, a little calculation gives

$$M_3 = \frac{(q-1)(7+18q+7q^2)}{640(q+1)^3} \quad (6)$$

in which $q \equiv l_2/l_1$, and this is independent of the total length of the body.

The asymmetry must be considered to be imperfectly resolved in the limit of vanishingly small $\mathcal{R}e$, but remains small until $\mathcal{R}e \gtrsim 25$, whereupon it grows linearly but slowly with $\mathcal{R}e$.

Fore-aft symmetry of the perfect projectile is expected in the case $\mathcal{R}e = 0$. For such flows, the pattern of streamlines around any body remains unchanged whether it travels forwards or backwards through the fluid: flow everywhere is perfectly reversed by reversal in the direction of body motion. The fluid drag is therefore the same

whether the body travel forward or backwards. Hence if we assume that the perfect projectile is unique, then it must have a fore-aft symmetric shape at $\mathcal{R}e = 0$. Our numerical experiments seem to exclude the possibility of multiple perfect projectiles, since searches starting from different initial shapes all ultimately converged upon the same drag-minimum.

We visualize the flow field and boundary stress upon a perfect projectile for $\mathcal{R}e = 50$ in Figure 2. Inertial effects give the flow two well-characterized asymmetric features [9]: vorticity generated at the boundary of the projectile remains confined within a thin boundary layer that grows with distance from the front of the body and is shed into an approximately paraboloidal wake behind the body. The stress field around the body is similarly asymmetric, with both viscous and pressure drag contributions largest in the extensional flow at the front of the body, and declining with distance from the front stagnation point. The high degree of flow asymmetry is not impressed upon the drag-minimizing body in a peculiar example of symmetry *un-breaking*: though the action (1) is asymmetric, its minimum is apparently symmetric.

III. SYMMETRY BREAKING IN WEAKLY INERTIAL FLOWS

Asymptotic study of the limit $\mathcal{R}e \rightarrow 0$ allows us to fortify our numerical results, which can not well-resolve the growth of asymmetry with Reynolds number below $\mathcal{R}e \approx 5$. The authors may as well admit that they believed that the symmetry of the perfect projectile would be broken at a finite value of $\mathcal{R}e$, mirroring the hierarchy of finite $\mathcal{R}e$ bifurcations that are seen in both steady and unsteady flows around bluff bodies, including the onset of boundary layer separation, breaking of symmetry in the vortex-wake and the transition from steady to unsteady vortex shedding. Our asymptotic study rules this out, showing that perfect projectiles have weak asymmetry all the way down to $\mathcal{R}e = 0$. We start by showing that leading order weak inertial effects are not sufficient for symmetry breaking.

A. Leading-order inertia effects do not break symmetry

We take a frame of reference co-moving with the body and identify the direction of the stream approaching the body with the z -direction. Upon non-dimensionalizing velocities \mathbf{u} by the far field velocity U , and lengths by the volumetric radius a , and stresses by $\eta U/a$, the flow field around the body may be seen to be governed by the steady Navier-Stokes equations:

$$\mathcal{R}e \mathbf{u} \cdot \nabla \mathbf{u} = -\nabla p + \nabla^2 \mathbf{u} \quad (7)$$

in addition to incompressibility $\nabla \cdot \mathbf{u} = 0$ and a no-slip boundary condition $\mathbf{u} = \mathbf{0}$ imposed upon the surface of

the body, and uniform stream $\mathbf{u} \rightarrow \hat{z}$, $p \rightarrow 0$ at infinity.

If inertial effects are weak (i.e. the Reynolds number is sufficiently small) then the leading-order effect of inertia upon the fluid drag encountered by the projectile can be effectively modeled by linearizing the left-hand side of (7) about the uniform stream to give Oseen's equation:

$$\mathcal{R}e \frac{\partial \mathbf{u}}{\partial z} = -\nabla p + \nabla^2 \mathbf{u} \quad \text{and} \quad \nabla \cdot \mathbf{u} = 0, \quad (8)$$

and this pair of equations can be solved by straightforward application of Green's function techniques [9].

However, Oseen's equation only properly approximates the Navier-Stokes equations at distances greater than $O(a/\mathcal{R}e)$ from the projectile. Closer to the body the perturbation to the uniform stream can not be said to be small. A more careful treatment of the low Reynolds number limit in which the Oseen approximation is matched to a regular perturbation expansion in the near field of the body [10]. From such treatments it can be shown that the Oseen equations correctly predict the $O(\mathcal{R}e)$ correction to the drag upon a projectile even though they do not correctly capture the pattern of streamlines [11, 12]. In the simplest case of a fore-aft symmetric body, it correctly gives the next correction to the symmetric component of the flow field, but adds anomalous antisymmetric flow components, which give no net contribution to the total drag experienced by the body.

We show that the drag predicted by the Oseen equations by the body is unaffected by the direction of travel of the body. To do this we denote by \mathbf{u} and $\hat{\mathbf{u}}$ the two flows set up when the incident flow approaches from the negative and positive z -directions respectively. Oseen's equations may be written in conservative form as $\nabla \cdot \mathbf{T} = \nabla \cdot \hat{\mathbf{T}} = \mathbf{0}$, if we define an effective stress tensor (which includes both viscous stresses and advection of momentum by the uniform stream): $\mathbf{T} \equiv -p\mathbf{1} + \nabla \mathbf{u} + (\nabla \mathbf{u})^T - \mathcal{R}e(\mathbf{u}\hat{z} + \hat{z}\mathbf{u})$. Then observe that:

$$\nabla \cdot (\boldsymbol{\sigma} \cdot \hat{\mathbf{u}} - \hat{\boldsymbol{\sigma}} \cdot \mathbf{u}) = \nabla \cdot (\mathcal{R}e(\mathbf{u} \cdot \hat{\mathbf{u}})\hat{z}), \quad (9)$$

or with a little manipulation

$$\nabla \cdot \left(\mathbf{T} \cdot \hat{\mathbf{u}} - \hat{\mathbf{T}} \cdot \mathbf{u} + \mathcal{R}e(\hat{z}\mathbf{u} \cdot \hat{\mathbf{u}} + \mathbf{u}\hat{u}_z + \hat{\mathbf{u}}u_z) \right) = 0, \quad (10)$$

now integrating the left-hand side over the entire of the fluid domain applying the divergence theorem, and carefully accounting for the rate of decay of the velocity field at infinity to eliminate the contributions from the far field we obtain the result: $\int_{\partial\Omega} \mathbf{n} \cdot (\boldsymbol{\sigma} + \hat{\boldsymbol{\sigma}}) \cdot \hat{z} dS = 0$, where the integration is taken over the boundary of the body $\partial\Omega$. It follows that the total drag force on the body is identical in magnitude but opposite in sign when the direction of the far field flow is reversed.

It follows that leading-order inertial effects, which can be modeled using Oseen's equations, are not sufficient to break the fore-aft symmetry of the projectile in the limit of $\mathcal{R}e \rightarrow 0$. Moreover, we note here our result shows that

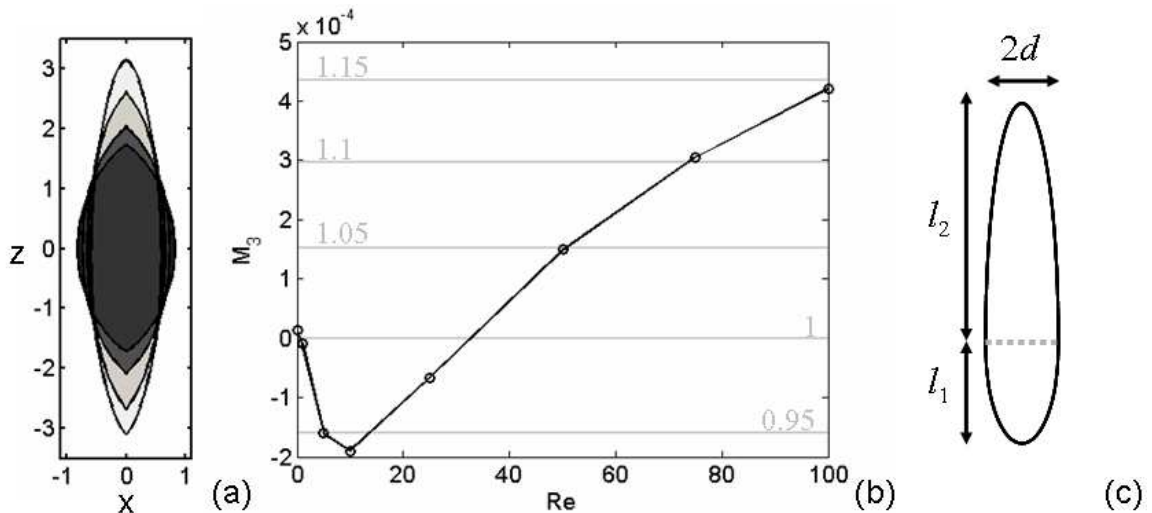


FIG. 1: (a) Minimum drag shapes evolved under a constant volume constraint. Key to shading: shapes computed for $Re = 0.1$ (darkest), $Re = 5.0$, $Re = 25.0$ and $Re = 100$ (lightest). Flow approaches each body from the negative z -direction. (b) Growth of the asymmetry parameter M_3 with Reynolds number. For comparison, the M_3 values for a reference body of controllable asymmetry (shown in figure (c)) are marked off. The number on each horizontal line reports the asymmetry ratio l_2/l_1 for the reference body. (c) Axisymmetric reference body used to generate the fiducial lines in panel (b). The reference body is formed by union of two spheroids of major axes l_1 , l_2 and common diameter $2d$.

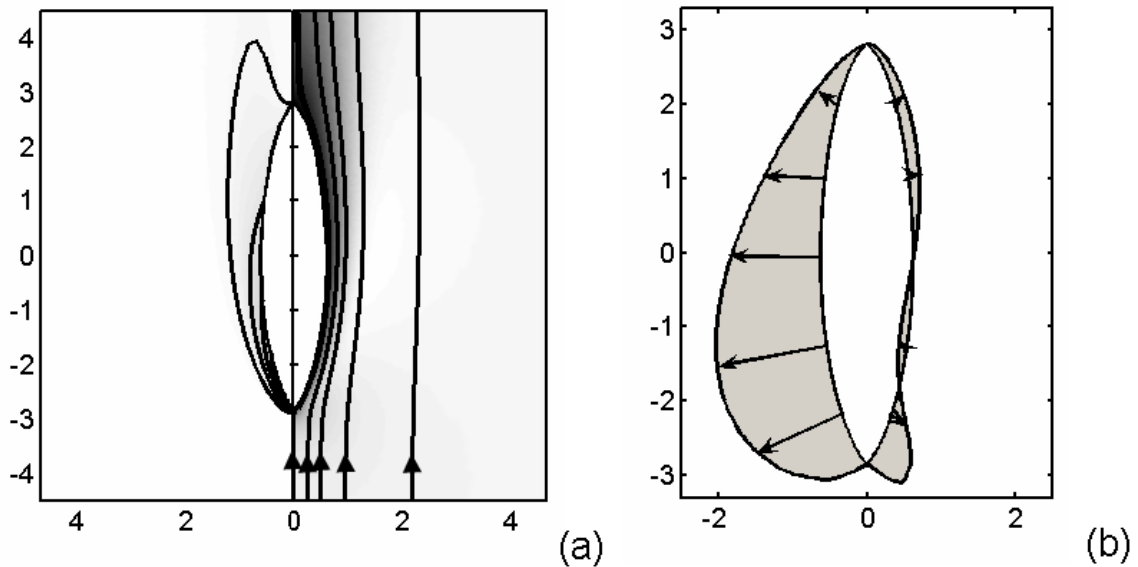


FIG. 2: Asymmetric flow field around a perfect projectile at $Re = 50$: (a) Left pane: vorticity contours. Right pane: streamlines (curves) and flow speed (shading). (b) Longitudinally integrated stress field plotted around the boundary of the perfect projectile. We separate the drag into (left pane) viscous shear stress and (right pane) pressure contributions.

the Oseen equations produce completely fore-aft symmetric perfect projectiles even when contributions at all order of Re are included. However we have no reason to expect the Oseen equation to accurately reproduce the drag upon the projectile beyond terms of $O(Re)$.

B. Fore-aft symmetry is broken at $O(Re^3)$

We show that inertial contributions up to $O(Re^3)$ must be included before the asymmetry of the perfect projectile becomes detectable. Our proof of this statement has

two halves: first we show that the drag upon an arbitrary body is unaffected when it's direction of travel is reversed, up to terms of $O(\mathcal{R}e^3 \log \mathcal{R}e)$. Then we show that contributions at $O(\mathcal{R}e^3)$ are sensitive to the direction of travel. We take an indirect route to this result by explicitly computing the first drag-minimizing step for a sphere, and showing that this step includes a non-symmetric component. Both calculations are somewhat lengthy, and we will consign the details to appendices. A physically motivated examination of the structure of the perturbation expansion explains the weak contribution of body asymmetry to drag.

Introduce a system of spherical polar coordinates (r, θ, ϕ) with $\theta = 0$ coinciding with the z -axis. We define a streamfunction, ψ , for the velocity field so that:

$$u_r = \frac{1}{r^2 \sin \theta} \frac{\partial \psi}{\partial \theta}, \quad u_\theta = -\frac{1}{r \sin \theta} \frac{\partial \psi}{\partial r}, \quad (11)$$

and follow Proudman and Pearson [10] by defining a transformed angle ordinate: $\beta \equiv \cos \theta$. The vorticity equation (formed by taking the curl of the Navier-Stokes equation (7)) may then be written in a form [10]:

$$\mathcal{E}_r^4 \psi = \mathcal{R}e \mathcal{H}_r[\psi, \psi], \quad (12)$$

in which we have defined operators:

$$\mathcal{E}_r^2 \equiv \frac{\partial^2}{\partial r^2} + \frac{1 - \beta^2}{r^2} \frac{\partial^2}{\partial \beta^2} \quad \text{and} \quad \mathcal{L}_r \equiv \frac{\beta}{1 - \beta^2} \frac{\partial}{\partial r} + \frac{1}{r} \frac{\partial}{\partial \beta}, \quad (13)$$

and

$$\mathcal{H}_r[\psi, \phi] \equiv \left(\frac{1}{r^2} \frac{\partial(\psi, \mathcal{E}_r^2 \phi)}{\partial(r, \beta)} + \frac{2}{r^2} \mathcal{E}_r^2 \phi \mathcal{L}_r \psi \right). \quad (14)$$

Equation (12) is supplemented by boundary conditions associated with regularity on the symmetry axis ($\psi = 0$ on $\beta = \pm 1$), no slip on the surface of the body ($\psi = (\mathbf{n} \cdot \nabla) \psi = 0$) and matching to the uniform stream at infinity ($\psi \rightarrow (1/2)r^2 \sin^2 \theta$ as $r \rightarrow \infty$).

In the limit of $\mathcal{R}e \rightarrow 0$, the flow field can be divided into two regions. There is a *Stokes layer* close to the body whose thickness scales with the size of the body, and an *Oseen layer* governing the flow at $O(1/\mathcal{R}e)$ distances from the body. In the Stokes layer the leading-order part of the vorticity equation represents a diffusive steady state attained as vorticity is introduced from some parts of the boundary of the body and eliminated at others. In the Oseen layer, we must introduce a rescaled length variable: $r = \lambda/\mathcal{R}e$ and streamfunction $\psi = \Psi/\mathcal{R}e^2$, $\mathcal{E}_r^2 = \mathcal{R}e^2 \mathcal{E}_\lambda^2$, and $\mathcal{L}_r = \mathcal{R}e \mathcal{L}_\lambda$. The vorticity equation takes the form

$$\mathcal{E}_\lambda^4 \Psi = \mathcal{H}_\lambda[\Psi, \Psi], \quad (15)$$

and the dominant balance in this layer features both diffusion of vorticity and advection by the uniform stream. Matching of the two solutions, Oseen and Stokes, imposes the condition that:

$$\lim_{\lambda \rightarrow 0} \Psi = \mathcal{R}e^2 \lim_{r \rightarrow \infty} \psi. \quad (16)$$

We seek an asymptotic expansion for the stream function within the Stokes region:

$$\psi = \psi_0 + \mathcal{R}e \psi_1 + \mathcal{R}e^2 \log \mathcal{R}e \psi_{2L} + \mathcal{R}e^2 \psi_2 + \mathcal{R}e^3 \log \mathcal{R}e \psi_{3L} + \mathcal{R}e^3 \psi_3 + O(\mathcal{R}e^4 \log^2 \mathcal{R}e) \quad (17)$$

and similarly within the Oseen region. At each step of the calculation, we find one new term in each of the Oseen and Stokes regions. Solution in both solutions contain arbitrary constants, corresponding to undetermined multiples of solutions to the homogeneous Stokes' and Oseen's equations. Matching the solutions in the two regions using (16) fixes the homogeneous components of the streamfunctions.

We pay particular attention to the form of the leading order streamfunction within the Stokes region, ψ_0 , which satisfies $\mathcal{E}_r^4 \psi_0 = 0$, and which at sufficiently large distances from the body $1 \ll r \ll \mathcal{R}e^{-1}$ may be expanded as a sum of multipole contributions, which we terminate after the force-octupole and source quadrupole contributions

$$\psi_0 = -\left(r^2 - \frac{1}{2}D_0 r + \frac{D_1}{r}\right) Q_1(\beta) + \left(C_0 + \frac{C_1}{r^2}\right) Q_2(\beta) + \frac{D_2}{r} Q_3(\beta) + \frac{C_2}{r^2} Q_4(\beta) + O\left(\frac{1}{r^3}\right). \quad (18)$$

Dependence upon meridional position is compactly expressed in terms of modified Gegenbauer polynomials; $Q_n(\beta) = \int_{-1}^{\beta} P_n(\beta') d\beta'$ [10]. Here we have distinguished between symmetric and antisymmetric contributions: $Q_{2n-1}(\beta) = Q_{2n-1}(-\beta)$ and $Q_{2n}(\beta) = -Q_{2n}(-\beta)$ so that all of the asymmetry of the flow is contained, to this order, in the $O(1)$ (stresslet) and $O(1/r^2)$ (source quadrupole and force octupole) contributions. More specifically, if the direction of flight of the projectile were to be reversed and new coordinates (r', β') defined in the same way (equivalent to reflecting the body in plane $z = 0$ so that the incident stream continues to approach from the negative z -direction) the new flow would be given by a streamfunction ψ^- , where at $O(1)$: $\psi^-(r', \beta') = \psi(r', -\beta')$, so that a multipole expansion for ψ^- would arrive at coefficients $C_m^- = -C_m$ and $D_m^- = D_m$. The Stokes drag force upon the particle is fixed by the strength of the $O(r)$ (Stokeslet) term: $F = 2\pi D_0$ [13, pages 133–138]. Moreover, by choice of our coordinate origin it is possible to eliminate the stresslet ($O(1)$) component of the streamfunction, permitting us to set $C_0 = 0$ without any loss of generality.

Our freedom to omit the stresslet term from the expansion of the streamfunction provides a route to establishing the absence of symmetry breaking below $O(\mathcal{R}e^3)$ without any further detailed calculation. Absent the stresslet term any fore-aft asymmetry in the shape of the projectile is communicated to an observer in the far-field only through force octupole and source quadrupole or weaker contributions to the flow field, giving a velocity field that decays like $O(1/r^4)$ or a contribution to the stress tensor that decays like $O(1/r^5)$. By contrast, the

strongest effect of the body is a Stokeslet velocity field that decays like $O(1/r)$, and leads to an $O(\mathcal{R}e)$ departure from the uniform stream in the Oseen layer. The $O(1/r^3)$ weaker asymmetric contribution to the multipole expansion leads to an $O(\mathcal{R}e^3)$ weaker correction to the flow in the Oseen layer (since the two flow fields must be matched on a sphere of $O(1/\mathcal{R}e)$ radius). The drag on the body can be extracted merely from determining the flow in the Oseen region, by enlarging the sphere on which the integral (33) is evaluated to some $1/\mathcal{R}e$ radius [14]. Since the contribution of projectile asymmetry to the flow field is only $O(\mathcal{R}e^4)$ within the Oseen region, the dependence of the drag upon such contributions will only be felt when $O(\mathcal{R}e^3)$ inertial effects are accounted for.

This argument glosses both the appearance of novel multipole terms among the higher order (in $\mathcal{R}e$) components of the streamfunction and the possibility of additional cancelations or symmetries that could allow the postponement of symmetry breaking effects to yet higher order in $\mathcal{R}e$. Excluding such effects requires the continuation of the asymptotic expansion up to terms of $o(\mathcal{R}e^3)$. We proceed with this calculation, although the uninterested reader will lose nothing by continuing directly to the Discussion section.

In order to determine higher order (in $\mathcal{R}e$) contributions to the streamfunction, it will turn out to be necessary to know the form of the streamfunction corresponding to placing the body in pure straining flow at infinity ($\psi_S \sim r^3 Q_2(\beta) + O(1)$ as $r \rightarrow \infty$), in addition to the streamfunction ψ_0 representing the slowly creeping flow around the body in a uniform stream. ψ_S includes no uniform flow terms proportional to $r^2 Q_1(\beta)$ (since these are forbidden by the far field conditions) or Stokeslet contribution (proportional to $r Q_1(\beta)$) since our choice of our choice of origin ensures that an axial straining flow exerts no force upon the body. For: in general, the force, torque and stresslet upon the particle are related to the flow fields imposed at infinity via a *grand-resistance matrix* [see ref. 15, pages 108–112], in particular for a uniform stream at infinity the stresslet exerted by the fluid upon the particle is given by

$$\mathbf{S} = \tilde{\mathbf{G}} \cdot \mathbf{U}^\infty, \quad (19)$$

and for uniform straining flow at infinity, the force upon the particle is given by:

$$\mathbf{F} = \mathbf{G} : \mathbf{E}^\infty. \quad (20)$$

Here \mathbf{G} and $\tilde{\mathbf{G}}$ are both rank 3 tensors, and it can be shown via the reciprocal theorem that $\tilde{G}_{ijk} = G_{kij}$. Thus by selecting our co-ordinates to eliminate the stresslet under uniform streaming conditions, we have ensured that $\tilde{G}_{ij3} = 0$, and thus guaranteed that under arbitrary symmetric straining flows there is no drag force upon the particle.

This set of observations gives us enough information to compute the drag force exerted by the fluid upon the

particle up to $O(\mathcal{R}e^2 \log \mathcal{R}e)$ corrections, simply by following the matching procedure developed by Proudman and Pearson [10].

The first two terms for the stream function within the Oseen layer can be shown to be:

$$\Psi_0 = \frac{1}{2} \lambda^2 (1 - \beta^2) \quad (21)$$

$$\Psi_1 = -\frac{D_0}{2} (1 + \beta) \left(1 - e^{-\lambda(1-\beta)/2} \right). \quad (22)$$

The $O(\mathcal{R}e)$ contribution to the streamfunction within the Stokes layer can be separated into a particular integral ψ_{1P} and a complementary function, which must be some multiple of ψ_0 , with the prefactor chosen to ensure that the matching condition is (16) satisfied up to terms of $O(r^2)$. We may additionally require of the particular integral that $\psi_{1P}^-(r', \beta') = -\psi_{1P}(r', -\beta')$. We may then make a multipole expansion of the solution:

$$\psi_1 \sim -\frac{C_3}{2} r Q_1 + \frac{D_0}{8} \left(r^2 - \frac{D_0}{2} r + D_3 \right) Q_2 + \frac{D_0}{8} \psi_0 + O\left(\frac{1}{r}\right). \quad (23)$$

where the coefficients (which transform to $D_3^- = D_3$ and $C_3^- = -C_3$ when the direction of flight is reversed) must be determined by applying the no slip condition upon the surface of body. Now D_3 is independent of whether the body moves forward or backwards and it can be shown that $C_3 = 0$: there is no Stokeslet contribution, because the drag suffered by the projectile is reversible up to $o(\mathcal{R}e)$ corrections [12].

The correction at $O(\mathcal{R}e^2)$ to the flow within the Oseen region is most easily obtained by Green's function techniques and has no simple closed form. However by careful asymptotic study of the integral expression it can be determined that as $\lambda \rightarrow 0$:

$$\begin{aligned} \Psi_2 \sim & \frac{\alpha_1}{2} \lambda (1 - \beta^2) - \frac{\alpha_1}{8} \lambda^2 (1 - \beta^2) (1 - \beta) \\ & + \frac{D_0^2}{32} \lambda \beta (1 - \beta^2) + \frac{D_0^2}{16} \lambda^2 (1 - \beta^2) \left(\frac{1}{5} \log \lambda + \frac{\gamma}{5} \right. \\ & \left. + \frac{1}{3} \log 2 - \frac{83}{200} - \frac{\beta}{8} + \frac{43}{1200} (5\beta^2 - 1) \right) \end{aligned} \quad (24)$$

up to $O(\lambda^3)$ corrections. Here γ is the Euler-Mascheroni constant and the coefficient α_1 (which corresponds to addition of a multiple of the homogenous solution Ψ_1) needs to be determined by application of the matching condition [16].

Proceeding to terms of $O(\mathcal{R}e^2)$ in the Stokes region we can construct a particular integral having three components:

$$\begin{aligned} \mathcal{E}_R^4 \psi_{2P1} &= \frac{D_0}{4} \mathcal{H}_r[\psi_0, \psi_0], \quad \mathcal{E}_R^4 \psi_{2P2} = \mathcal{H}_r[\psi_{1P}, \psi_0] \\ &\text{and} \quad \mathcal{E}_R^4 \psi_{2P3} = \mathcal{H}_r[\psi_0, \psi_{1P}]. \end{aligned} \quad (25)$$

Clearly we may take $\psi_{2P1} = \frac{D_0}{4} \psi_{1P}$, and demand that the other components have the reversal property $\psi_{2P2}^-(r', \beta') = \psi_{2P2}(r', -\beta')$ and $\psi_{2P3}^-(r', \beta') =$

$\psi_{2P3}(r', -\beta')$. To this we must add a multiples of our two homogeneous solutions ψ_0 and ψ_S . The the solution within the Stokes layer can be shown to have the form

$$\begin{aligned} \psi_2 = & \left(\frac{D_0 r^3}{40} - \frac{D_0^2 r^2 \log r}{40} + D_4 R \right) Q_1 + \frac{D_0^2 r^2}{32} Q_2 \\ & + \left(\frac{D_0 r^3}{60} - \frac{43 D_0^2 r^2}{2400} \right) Q_3 + A_1 \psi_0 + B_1 \psi_S + O(\mathcal{R}e^{-2}) \end{aligned} \quad (26)$$

with the constants A_1 and B_1 and the unknown constant α_1 that appears in the Oseen layer solution all chosen to satisfy the matching condition (16) at $O(r^3)$:

$$\begin{aligned} \alpha_1 = -\frac{D_0^2}{16}, \quad A_1 = -D_0^2 \left(\frac{29}{800} - \frac{\gamma}{40} - \frac{1}{24} \log 2 \right) \\ \text{and} \quad B_1 = -\frac{D_0}{24}. \end{aligned} \quad (27)$$

Notice that on matching to the Oseen layer solution on a sphere of radius $O(1/\mathcal{R}e)$, we appear to pick up a uniform stream contribution at $O(\mathcal{R}e^2 \log \mathcal{R}e)$. Demonstrably, no such terms appear in the Oseen layer expansion, so it is necessary to introduce a canceling term at intermediate order in the perturbation expansion:

$$\psi_{2L} = \frac{D_0^2}{40} \psi_0. \quad (28)$$

The appearance of a term of this order forces the introduction of terms at $O(\mathcal{R}e^3 \log \mathcal{R}e)$ in both Stokes and Oseen layers, having respective forms

$$\psi_{3L} \sim A_2 \psi_0 + \frac{D_0^3}{160} \left(r^2 - \frac{D_0}{2} r \right) Q_2 + O\left(\frac{1}{r}\right) \quad (29)$$

$$\Psi_{3L} = \alpha_2 (1 + \beta) \left(1 - e^{-\lambda(1-\beta)/2} \right), \quad (30)$$

and in order to match with to the Oseen solution, it is also necessary to isolate the far-field contribution of size $r^2 \log r$ arising from ψ_3

$$\psi_3 = \dots - \frac{3D_0^3}{320} r^2 (\log r) Q_1 + \dots, \quad (31)$$

matching gives $\alpha_2 = -D_0^3/80$ and $A_2 = D_0^3/80$.

We now have sufficiently many terms to be able to compute the drag (D) upon the body up to $O(\mathcal{R}e^3 \log \mathcal{R}e)$ contributions. Note that, similar to the Oseen equations, the Navier-Stokes equations may be written in a conservative form

$$\nabla \cdot \boldsymbol{\tau} = \mathbf{0} \quad \text{where} \quad \boldsymbol{\tau} = -p\mathbf{1} + (\nabla \mathbf{u} + (\nabla \mathbf{u})^T) - \mathcal{R}e \mathbf{u} \mathbf{u}. \quad (32)$$

By appealing to the divergence theorem we may then convert the integral of the surface stress around the body to an integration around a sphere of very large (but nonetheless $\ll 1/\mathcal{R}e$) radius:

$$D = \int_S \mathbf{n} \cdot \boldsymbol{\tau} \cdot \hat{\mathbf{z}} dS = - \int_{S_\infty} \mathbf{n} \cdot \boldsymbol{\tau} \cdot \hat{\mathbf{z}} dS = F_p + F_s + F_m, \quad (33)$$

in which \mathbf{n} is the outward pointing normal on S , and equal to $-\mathbf{e}_r$ on S_∞ . We have separated the integral into three distinct contributions, a contribution from the *pressure* force:

$$F_p = - \int_{S_\infty} p \cos \theta dS = \pi \int_{-1}^1 \frac{\partial p}{\partial \theta} (1-\beta^2)^{1/2} r^2 d\beta, \quad (34)$$

where $\partial p/\partial \theta$ may be read directly off from the meridional component of the Navier-Stokes equation, plus a contribution from *viscous* stresses:

$$\begin{aligned} F_s = 2\pi \int_{-1}^1 \left[2 \frac{\partial u_r}{\partial r} \beta - (1-\beta^2)^{1/2} \left(\frac{\partial u_\theta}{\partial r} - \frac{u_\theta}{r} \right. \right. \\ \left. \left. - \frac{(1-\beta^2)^{1/2}}{r} \frac{\partial u_r}{\partial \beta} \right) \right] r^2 d\beta, \end{aligned} \quad (35)$$

and a contribution from *transport of momentum* through the surface S_∞ :

$$F_m = -2\pi \int_{-1}^1 u_r \left(u_r \beta - u_\theta (1-\beta^2)^{1/2} \right) r^2 d\beta. \quad (36)$$

Summing these three contributions for some $O(1/\mathcal{R}e)$ value of r we arrive at an expression relating the total drag upon the body to the coefficients of the multipole expansion for the Stokes layer stream function:

$$\begin{aligned} \frac{D}{D_S} = 1 + \frac{D_0}{8} \mathcal{R}e + \frac{D_0^2}{40} \mathcal{R}e^2 \log \mathcal{R}e \\ + \left(D_0^2 \left(\frac{\log 2}{24} + \frac{\gamma}{40} - \frac{13}{600} \right) + \frac{D_3}{20} + \frac{2D_4}{D_0} \right) \mathcal{R}e^2 \\ + \frac{D_0^3}{80} \mathcal{R}e^3 \log \mathcal{R}e + O(\mathcal{R}e^3), \end{aligned} \quad (37)$$

here we have followed Chester and Breach [16] by scaling the total drag force upon the projectile by the Stokes drag ($D_S = 2\pi D_0$). Note that all of the coefficients that appear in this expression remain invariant when the direction of flight is reversed: the terms appearing in the streamfunction for reversed flow ψ^- are identical to their counterparts in ψ : $D_m^- = D_m$. It follows that up to $O(\mathcal{R}e^3)$ contributions the drag upon the projectile is independent of whether it travels backwards or forwards through the fluid.

It is therefore possible to determine, up to $O(\mathcal{R}e^3 \log \mathcal{R}e)$ inertial corrections, the symmetry or anti-symmetry of all of the $O(1/r)$ components of the velocity field around an arbitrary axisymmetric projectile under reversal of its direction of flight. The drag upon the projectile may be explicitly related to these velocity field components, and shown to in fact depend only upon the symmetric components. Antisymmetric flow field components start to contribute to the drag upon the projectile when $O(\mathcal{R}e^3)$ inertial corrections are included.

We show that $O(\mathcal{R}e^3)$ contributions to the drag are altered by reversal in the direction of travel of the projectile by direct computation of the first step made if

the drag-minimizing algorithm is started with a spherical body. The drag-minimizing step includes an antisymmetric component, which we exhibit. In order to do this, we construct an analogue of the vorticity equation for the adjoint field \mathbf{w} , by introducing a flux-function ϕ so that

$$w_r = \frac{1}{r^2 \sin \theta} \frac{\partial \phi}{\partial \theta}, \quad w_\theta = -\frac{1}{r \sin \theta} \frac{\partial \phi}{\partial r}. \quad (38)$$

By taking the curl of the adjoint equation (2) we arrive at

$$-\mathcal{E}_r^4 \phi = \mathcal{R}e \mathcal{H}_r[\phi, \psi] + \mathcal{R}e \mathcal{E}_r^2 \left(\frac{\partial(\psi, \phi)}{\partial(r, \beta)} \right), \quad (39)$$

and this equation can be analyzed in the limit $\mathcal{R}e \rightarrow 0$ in the same manner as the vorticity equation (32). Sufficient information about the velocity streamfunction ψ is provided by the earlier analysis of Chester and Breach [16]. Just as for the vorticity equation (12) it is necessary to separate the flow field into Stokes and Oseen layers, which entails rescaling the flux-function and radial coordinate for the Oseen layer.

Within the Oseen region, the leading order flow is a uniform stream directed in the opposite sense to the physical flow around the body:

$$\Phi_0(\lambda, \beta) = -\frac{1}{2} \lambda^2 (1 - \beta^2). \quad (40)$$

Picking out terms of $O(\mathcal{R}e)$ from (39) gives

$$\mathcal{E}_\lambda^2 (\mathcal{E}_\lambda^2 \Phi_1 + (1 - \beta^2) \mathcal{L}_\lambda \Phi_1) = 0, \quad (41)$$

which is identical to Oseen's equation with the direction of far field advection reversed. The resemblance to the physical flow field enables us to write down the second term in the perturbation expansion of Φ

$$\Phi_1(\lambda, \beta) = -\Psi_1(\lambda, -\beta) = -\frac{3}{2} (1 - \beta) (1 - e^{-\lambda(1+\beta)/2}), \quad (42)$$

while similar treatment of (39) within the Stokes region

yields

$$\begin{aligned} \phi_0(r, \beta) &= -\psi_0(r, -\beta) = \left(r^2 - \frac{3r}{2} + \frac{1}{2r} \right) Q_1(\beta) \\ \phi_1(r, \beta) &= -\psi_1(r, -\beta) = \frac{3}{8} \left(r^2 - \frac{3r}{2} + \frac{1}{2r} \right) Q_1(\beta) \\ &\quad + \frac{3}{16} \left(2r^2 - 3r + 1 - \frac{1}{r} + \frac{1}{r^2} \right) Q_2(\beta) \end{aligned} \quad (43)$$

Evaluating $O(\mathcal{R}e^2)$ contributions within the Oseen layer, we arrive at an equation

$$\begin{aligned} \mathcal{E}_\lambda^2 (\mathcal{E}_\lambda^2 \Phi_2 + (1 - \beta^2) \mathcal{L}_\lambda \Phi_2) &= \\ -H_\lambda[\Phi_1, \Psi_1] - \mathcal{E}_\lambda^2 \left(\frac{1}{\lambda^2} \frac{\partial(\Psi_1, \Phi_1)}{\partial(\lambda, \beta)} \right) &= 0. \end{aligned} \quad (44)$$

We follow Chester and Breach [16] by solving this equation using Green's function techniques, consigning the details of the calculation to Appendix A. Application of the flux function version of the matching condition (16) and asymptotic study of our Green's function solution produces:

$$\begin{aligned} \Phi_2(r, \beta) &\sim \left(\frac{9\beta}{32} + \frac{9}{32} \right) \lambda (1 - \beta^2) + \frac{9}{64} \left(\frac{359}{100} - \frac{8}{5} \log \lambda \right. \\ &\quad \left. - \frac{8}{5} \gamma - \frac{8}{3} \log 2 - \frac{1}{2} \beta - \frac{11}{60} \beta^2 - \frac{1}{2} (1 + \beta) \right) \\ &\quad \times \lambda^2 (1 - \beta^2). \end{aligned} \quad (45)$$

Matching to this solution then gives us enough boundary conditions to completely solve for the adjoint field within the Stokes region:

$$\begin{aligned} \mathcal{E}_r^4 \phi_2 &= -\mathcal{H}_r[\phi_0, \psi_1] - \mathcal{H}_r[\phi_1, \psi_0] \\ &\quad - \mathcal{E}_r^2 \left(\frac{1}{r^2} \frac{\partial(\psi_0, \phi_1)}{\partial(r, \beta)} + \frac{1}{r^2} \frac{\partial(\psi_1, \phi_0)}{\partial(r, \beta)} \right) \end{aligned} \quad (46)$$

from which we deduce

$$\begin{aligned} \phi_2 &= \left[\frac{9}{640} \left(-\frac{16r^3}{3} + 32r^2 \log r + 24r \log r - \frac{287r}{15} + 1 + \frac{8 \log r}{5r} + \frac{1111}{45r} - \frac{1}{r^2} - \frac{2}{3r^3} + \frac{4}{9r^4} \right) \right. \\ &\quad \left. + \frac{3}{4} \left(\log 2 + \frac{3\gamma}{5} - \frac{229}{200} \right) \left(r^2 - \frac{3r}{2} + \frac{1}{r} \right) \right] Q_1 \\ &\quad + \left[\frac{9}{64} \left(2r^2 - 3r + 1 - \frac{1}{r} + \frac{1}{r^2} \right) + \frac{5}{40} \left(r^3 - \frac{5}{2} + \frac{3}{2r^2} \right) \right] Q_2 \\ &\quad + \frac{9}{320} \left(-\frac{16r^3}{9} + \frac{22r^2}{15} - \frac{14r}{15} + \frac{16}{3} - \frac{8 \log r}{35r} - \frac{573}{70r} + \frac{8}{r^2} - \frac{2669}{630r^3} + \frac{1}{3r^4} \right) Q_3. \end{aligned} \quad (47)$$

Additionally, because there is no term at $O(\mathcal{R}e \log \mathcal{R}e)$

in the Oseen-region expansion, we must introduce an ad-

ditional term at $O(\mathcal{R}e^2 \log \mathcal{R}e)$ for matching:

$$\phi_{2L} = \frac{9}{20} \left(r^2 - \frac{3r}{2} + \frac{1}{2r} \right) Q_1 . \quad (49)$$

In order to determine the effect of $O(\mathcal{R}e^3)$ inertial terms upon the first drag-minimizing step we must solve for both the streamfunction and adjoint flux-function, since the analysis of Chester and Breach [16] does not

extend to this order. It suffices for demonstration that symmetry is indeed broken to compute the Q_3 and Q_4 components of both of these functions. In order to calculate the Q_2 -component of the stream function we would need to extend the expansion of Ψ_2 up to $O(\lambda^3)$, and in order to compute the Q_1 -component, we would need to make a lengthy asymptotic study of Ψ_3 . For the streamfunction ψ we obtain

$$\begin{aligned} \psi_3 = \dots &+ \left[\frac{9}{640} \left(\frac{16r^3}{3} - \frac{129r^2}{10} + \frac{377r}{18} - \frac{76}{3} + \frac{32621}{2520r} + \frac{144 \log r}{35r} - \frac{221}{36r^2} + \frac{12977}{2520r^3} + \frac{6 \log r}{7r^3} \right) \right. \\ &- \left. \frac{3}{160} \left(r^3 - \frac{7}{2r} + \frac{5}{2r^3} \right) \right] Q_3 \\ &+ \frac{3}{224} \left(\frac{5r^4}{3} - \frac{67r^3}{7} + \frac{677r^2}{30} - \frac{237r}{8} + \frac{24 \log r}{7} + \frac{2627}{112} - \frac{72 \log r}{7r} - \frac{821}{336r} + \frac{45 \log r}{28r^2} \right. \\ &- \left. \frac{640019}{73920r^2} + \frac{211}{32r^3} - \frac{39 \log r}{14r^3} - \frac{155 \log r}{132r^4} - \frac{306839}{73920r^4} + \frac{1}{6r^5} \right) Q_4 . \end{aligned} \quad (50)$$

In order to compute the contribution at $O(\mathcal{R}e^3 \log \mathcal{R}e)$ we must also extract all of the terms proportional to $r^2 \log r$ from ψ_3 and this can be done without knowing the full functional form of the Q_1 and Q_2 components:

$$\psi_3 = \dots + \frac{9}{80} r^2 \log r \left(-\frac{9}{4} Q_1 + Q_2 \right) + \dots \quad (51)$$

We can also solve the $O(\mathcal{R}e^3 \log \mathcal{R}e)$ problem directly to arrive at [16]:

$$\begin{aligned} \psi_{3L} = d \left(r^2 - \frac{3r}{2} + \frac{1}{2r} \right) Q_1 \\ + \frac{27}{160} \left(r^2 - \frac{3r}{2} + \frac{1}{2} - \frac{1}{2r} + \frac{1}{2r^2} \right) Q_2 , \end{aligned} \quad (52)$$

with d an unknown constant that must be deduced from matching to the Oseen layer solution:

$$\Psi_{3L} = D(1 + \beta) \left(1 - e^{-\lambda(1-\beta)/2} \right) . \quad (53)$$

Application of the matching condition (16) then gives $d = -\frac{27}{320}$ and $D = -\frac{27}{80}$ [16].

A similar sequence of steps allows us to pick out the $O(\mathcal{R}e^3 \log \mathcal{R}e)$ contributions to the adjoint flux-function:

$$\begin{aligned} \phi_3 = \dots &+ \left[\frac{3}{40} \left(r^3 - \frac{387r^2}{160} + \frac{377r}{96} - \frac{19}{4} + \frac{27 \log r}{35r} + \frac{32621}{13440r} - \frac{221}{192r^2} - \frac{9 \log r}{56r^3} \right. \right. \\ &+ \left. \left. \frac{12977}{13440r^3} \right) + \frac{3}{160} \left(r^4 - \frac{7}{2r} + \frac{5}{2r} \right) \right] Q_3 + \frac{1}{31360} \left(140r^4 - 132r^3 + \frac{511r^2}{5} \right. \\ &- \frac{1323r}{2} + 36 \log r + \frac{31989}{20} - \frac{486 \log r}{r} - \frac{3269}{2r} + \frac{1911443}{880r^2} - \frac{495 \log r}{r^2} \\ &- \left. \frac{109857}{40r^3} + \frac{2835 \log r}{11r^4} + \frac{1101527}{880r^4} + \frac{12 \log r}{r^5} - \frac{503}{5r^5} + \frac{105}{11r^6} \right) Q_4 . \end{aligned} \quad (54)$$

In order to determine ϕ_{3L} , we isolate the component of

the adjoint flux-function that varies with r as $r^2 \log r$:

$$\phi_3 = \dots + \frac{81r^2 \log r}{160} Q_1 + \dots \quad (55)$$

matching then yields

$$\begin{aligned} \phi_{3L} = & \frac{6561}{51200} \left(r^2 - \frac{3r}{2} + \frac{1}{2r^2} \right) Q_1 \\ & + \frac{81}{320} \left(r^2 - \frac{3r}{2} + \frac{1}{2} - \frac{1}{2r} + \frac{1}{2r^2} \right) Q_2. \end{aligned} \quad (56)$$

In terms of the stream- and flux- functions the (dimensional) shape derivative (4) takes a form:

$$\alpha \propto \left(\frac{\eta U^2}{a^2} \right) \left(-\frac{\mathcal{E}_r^2 \psi \mathcal{E}_r^2 \phi}{r^2 \sin^2 \theta} + \left\langle \frac{\mathcal{E}_r^2 \psi \mathcal{E}_r^2 \phi}{r^2 \sin^2 \theta} \right\rangle \right). \quad (57)$$

Inputting our expansions for ϕ and ψ we see that asymmetric terms start to appear in this expression only at $O(\mathcal{R}e^3)$, and include (in addition to a Q_2 component that we have not determined) a term that provides the requisite symmetry breaking effect:

$$\alpha_{\text{a.s.}} = \frac{952431}{2759680} \mathcal{R}e^3 Q_4 \quad (58)$$

IV. DISCUSSION

We have presented a surprising property of perfect projectiles – bodies of prescribed volume that are shaped to experience the minimum possible drag when traveling steadily through a fluid – although the flow around such bodies becomes markedly asymmetric at moderate Reynolds numbers, the projectiles themselves remain quite fore-aft symmetric.

We have shown, by asymptotic study of the Navier-Stokes drag upon an arbitrarily shaped projectile, that there are small ($O(\mathcal{R}e^3)$) asymmetries in the perfect projectile shape even in the limit of arbitrarily weak inertia. However the persistence of near-symmetry up to moderate Reynolds numbers remains unexplained.

One possible explanation for the symmetry “un-breaking” is provided by our study of the Oseen equations. We have shown that under the Oseen approximation, the drag upon a projectile is independent of its degree of asymmetry; perfect projectiles in Oseen flow remain exactly fore-aft symmetric up to arbitrarily large Reynolds numbers. It has previously been shown that *weak* ($O(\mathcal{R}e)$) inertial corrections to the drag upon a moving body are independent of whether it moves forward or backward through the fluid [12, 17]. Because of this, such weak corrections may be directly computed by solving Oseen’s equations throughout the entire of the fluid-filled domain, allowing the different physical balances that operate within Stokes and Oseen layers to be overlooked [11]. We postulate that the drag-determining features of the Navier-Stokes equations up to *moderate* Reynolds numbers can similarly be captured, by an approximation that has the same features of linearity and

reciprocity under reversal in the direction of flight as Oseen’s equations.

One candidate set of equations with these properties has been proposed by Carrier [18], who sought an approximation that correctly captured the flow-field within the immediate neighborhood of the body and in the far field without requiring fidelity at intermediate scales. He fastened upon a variant of the Oseen approximation in which the Reynolds number featuring in the Oseen equations (8) is allowed to differ from the value that is put into the Navier-Stokes equations. By fitting to experimental data Carrier determined that setting $\mathcal{R}e_O = 0.43\mathcal{R}e_{NS}$ gives fairly good accord for the steady fluid drag upon flat plates, spheres and cylinders from $\mathcal{R}e_{NS} = 5$ up to around 20.

The persistence of near-symmetry in perfect projectiles up to much larger Reynolds numbers than this is indirect evidence that if we consider a broader class of possible dependencies of $\mathcal{R}e_O$ upon $\mathcal{R}e_{NS}$ then an approximation in the same spirit may correctly render the drag-determining features of the flow. This regime of Reynolds numbers, which spans a number of flow transitions including the onset of vortex shedding from a bluff body and breaking of wake symmetry, has been notoriously inaccessible to asymptotic study [9, page 327], and linearity and reciprocity under flow reversal must hitherto have been considered severe impediments to any theory that aspires to capture the drag-determining characters of the flow. Modifications of Oseen’s equation provide us with a new way of thinking about flow in this most difficult of regimes and we discuss their strengths and limitations more fully in a follow-up paper.

Although the mechanisms underlying the persistence of near-symmetry in the shape of the perfect projectile require additional elucidation, fore-aft symmetry provides us with one robust, though unexpected, signature of drag-minimization against which the bauplans of small, rapidly moving, bioprojectiles may be compared.

Acknowledgments

The work was supported by the Kao and Kodak Fellowships and by the NSF Division of Mathematical Sciences. Discussions with Howard Stone are gratefully acknowledged.

APPENDIX A: SENSITIVITY OF DRAG TO DIRECTION OF FLIGHT AT $O(\mathcal{R}e^3)$

In order to fully compute the adjoint flux-function ϕ_2 within the Stokes layer we must solve, in the limit as $\lambda \rightarrow 0$ for the corresponding Oseen flux-function from

$$\begin{aligned}
\mathcal{E}_\lambda^2 (\mathcal{E}_\lambda^2 \Phi_2 + (1 - \beta^2) \mathcal{L}_\lambda \Phi_2) &= -H_\lambda[\Phi_1, \Psi_1] - \mathcal{E}_\lambda^2 \left(\frac{1}{\lambda^2} \frac{\partial(\Psi_1, \Phi_1)}{\partial(\lambda, \beta)} \right) \\
&= \frac{9}{16\lambda^4} (1 - \beta^2) \left[-e^{-\lambda(1+\beta)/2} (8 + 4\lambda(1 + 2\beta) + \lambda^2(1 + \beta)) \right. \\
&\quad + 2e^{-\lambda(1-\beta)/2} (2 + \lambda(1 + 3\beta)) \\
&\quad \left. + e^{-\lambda} (4 + 4\lambda(1 + 2\beta) + \lambda^2(3 + 5\beta) + \lambda^3(1 + \beta)) \right] . \tag{A1}
\end{aligned}$$

We follow Chester and Breach [16] by solving this equation using Green's function techniques. Specifically, if we

abbreviate the righthand side of (A1) by $F(\lambda, \theta)$, then a particular solution to the equation may be written as:

$$\begin{aligned}
\Phi_2(\lambda, \theta) &= -\frac{\lambda \sin \theta}{4\pi} \int_0^\infty \int_0^\pi \int_0^{2\pi} \lambda_1 \cos \varphi_1 d\lambda_1 d\theta_1 d\varphi_1 F(\lambda_1, \theta_1) \\
&\quad \times \int_0^{\frac{1}{2}[(\lambda_1^2 + \lambda^2 - 2t\lambda\lambda_1)^{1/2} + \lambda \cos \theta - \lambda_1 \cos \theta_1]} \frac{1 - e^{-\alpha}}{\alpha} d\alpha \tag{A2}
\end{aligned}$$

where we have defined

$$t \equiv \cos \theta \cos \theta_1 + \sin \theta \sin \theta_1 \cos \varphi_1 . \tag{A3}$$

Now in order to approximate this integral in the limit of $\lambda \rightarrow 0$, we carve the integration domain into two regions: a near field $0 < \lambda_1 < k$ and far field $\lambda_1 > k$ where we impose a separation of scales $\lambda \ll k \ll 1$.

In the *near field* we may approximate:

$$\int_0^\mu \frac{1 - e^{-\alpha}}{\alpha} d\alpha = \mu - \frac{1}{4}\mu^2 + O(\mu^3) , \tag{A4}$$

where we have defined a place-holder variable $\mu \equiv \frac{1}{2} [(\lambda_1^2 + \lambda^2 - 2t\lambda\lambda_1)^{1/2} + \lambda \cos \theta - \lambda_1 \cos \theta_1]$. We can then greatly simplify the work required for the evaluation of the integral by noting that

$$\begin{aligned}
&\int_0^{2\pi} (\lambda_1^2 + \lambda^2 - 2t\lambda\lambda_1) \cos \varphi_1 d\varphi_1 = \\
&\quad - \int_0^{2\pi} 2\lambda\lambda_1 \sin \theta \sin \theta_1 \cos^2 \varphi_1 d\varphi_1 \tag{A5}
\end{aligned}$$

while

$$\begin{aligned}
&\int_0^{2\pi} (\lambda_1^2 + \lambda^2 - 2t\lambda\lambda_1)^{1/2} \cos \varphi_1 d\varphi_1 = \\
&\quad - \int_0^{2\pi} \frac{\lambda\lambda_1 \sin \theta \sin \theta_1}{(\lambda_1^2 + \lambda^2 - 2t\lambda\lambda_1)^{1/2}} \sin^2 \varphi_1 d\varphi_1 , \tag{A6}
\end{aligned}$$

on integrating by parts. Thus the near field integral may be approximated as:

$$\begin{aligned}
\Phi_2^{(n)}(\lambda, \theta) &= \frac{\lambda^2 \sin^2 \theta}{8\pi} \int_0^k \int_0^\pi \int_0^{2\pi} \lambda_1^2 \sin \theta_1 \sin^2 \varphi_1 d\lambda_1 d\theta_1 d\varphi_1 \frac{F_1(\lambda_1, \theta_1)}{(\lambda_1^2 + \lambda^2 - 2t\lambda\lambda_1)^{1/2}} \\
&\quad \times \left(1 - \frac{1}{4} [(\lambda_1^2 + \lambda^2 - 2t\lambda\lambda_1)^{1/2} + \lambda \cos \theta - \lambda_1 \cos \theta_1] \right) , \tag{A7}
\end{aligned}$$

we may moreover make a small argument approximation to $F(\lambda_1, \theta_1)$:

$$\begin{aligned}
F(\lambda_1, \theta_1) &= \sin^2 \theta_1 \left[\frac{27}{4\lambda_1^3} \cos \theta_1 \right. \\
&\quad \left. + \frac{9}{32\lambda_1^2} (1 - 6 \cos \theta_1 + 13 \cos^2 \theta_1) \right] \tag{A8}
\end{aligned}$$

in which we have retained terms up to $O(1/\lambda_1)$.

Picking a typical term: in order to evaluate the leading order contribution (at $O(\lambda)$) to $\Phi_2^{(n)}$ we must compute:

$$\Phi_2^{(n,1)}(\lambda, \theta) = \left(\frac{27\lambda^2 \sin^2 \theta}{8} \right) \frac{1}{4\pi} \int_0^k \int_0^\pi \int_0^{2\pi} \frac{1}{\lambda_1} d\lambda_1 d\theta_1 d\varphi_1 \times \frac{\sin^3 \theta_1 \cos \theta_1 \sin^2 \varphi_1}{(\lambda_1^2 + \lambda^2 - 2t\lambda\lambda_1)^{1/2}} \quad (\text{A9})$$

and (omitting the prefactor in parenthesis) we recognize this to be the Green's function solution to Poisson's equation

$$\nabla^2 \chi = -\frac{1}{\lambda^3} \sin^2 \theta \cos \theta \sin^2 \varphi, \quad (\text{A10})$$

evaluated at $\varphi = 0$. It is not difficult to solve this equation by decomposing the forcing function into a sum of

spherical harmonics:

$$\chi = \frac{1}{\lambda} \left(\frac{1}{5} \sqrt{\frac{\pi}{3}} Y_1^0 - \frac{1}{12} \sqrt{\frac{2\pi}{105}} Y_3^{-2} - \frac{1}{30} \sqrt{\frac{\pi}{7}} Y_3^0 - \frac{1}{12} \sqrt{\frac{2\pi}{105}} Y_3^2 \right) + O(\lambda) \quad (\text{A11})$$

for $\lambda < k$. Thus

$$\Phi_2^{(n,1)}(\lambda, \theta) = \frac{9}{32} \lambda \sin^2 \theta \cos \theta, \quad (\text{A12})$$

and we may compute the other integrals that arise from expanding the sum (A7) by the same method:

$$\Phi_2^{(n)}(\lambda, \theta) = \frac{9}{32} \lambda \sin^2 \theta \cos \theta + \frac{9}{128} \left(\frac{16}{5} \log \left(\frac{k}{\lambda} \right) + \frac{127}{50} - \cos \theta - \frac{11}{30} \cos^2 \theta \right) \lambda^2 \sin^2 \theta, \quad (\text{A13})$$

In the *far field* we instead approximate:

$$\int_0^\mu \frac{1 - e^{-\alpha}}{\alpha} d\alpha = \int_0^{\frac{\lambda_1}{2}(1 - \cos \theta_1)} \frac{1 - e^{-\alpha}}{\alpha} d\alpha - \lambda(t - \cos \theta) \frac{\left(1 - e^{-\frac{\lambda_1}{2}(1 - \cos \theta_1)} \right)}{\frac{\lambda_1}{2}(1 - \cos \theta_1)} \quad (\text{A14})$$

continuing our expansion as far as terms of $O(\lambda_1^2)$. When the φ_1 integration is performed we are left with a single non-vanishing contribution

$$\Phi_2^{(f)} = \frac{\lambda^2 \sin^2 \theta}{4} \int_k^\infty \int_0^\pi d\lambda_1 d\theta_1 (1 + \cos \theta_1) \times \left(1 - e^{-\frac{\lambda_1}{2}(1 - \cos \theta_1)} \right) \frac{F(\lambda_1, \theta_1)}{\sin \theta_1}. \quad (\text{A15})$$

This integral may be directly evaluated in the limit of $k \rightarrow 0$, yielding:

$$\Phi_2^{(f)}(\lambda, \theta) \sim -\frac{\lambda^2 \sin^2 \theta}{4} \left(\frac{9}{10} \log k + \frac{3}{2} \log 2 + \frac{9}{10} \gamma - \frac{261}{200} \right), \quad (\text{A16})$$

up to terms of $O(\lambda^3)$. Finally, we may also add an arbitrary multiple of the solution to the homogeneous equation

$$\Phi_2^{(h)}(\lambda, \theta) = C(1 - \beta)(1 - e^{-\lambda(1+\beta)/2}), \quad (\text{A17})$$

and combining these three expressions then gives us:

$$\Phi_2(r, \beta) \sim \left(\frac{9\beta}{32} + \frac{C}{2} \right) \lambda(1 - \beta^2) + \frac{9}{64} \left(\frac{359}{100} - \frac{8}{5} \log \lambda - \frac{8}{5} \gamma - \frac{8}{3} \log 2 - \frac{1}{2} \beta - \frac{11}{60} \beta^2 - \frac{8C}{9}(1 + \beta) \right) \lambda^2(1 - \beta^2) \quad (\text{A18})$$

By matching with the Stokes layer expansion at $O(r)$ we infer that $C = \frac{9}{16}$, which completes our derivation of the equation (46).

- [1] S. Vogel, "Living in a physical world II. The bio-ballistics of small projectiles," *J. Biosci.* pp. 167–175 (2005).
 [2] S. Vogel, *Life in Moving Fluids: The Physical Biology of Flow* (Princeton University Press, 1994), 2nd ed.

- [3] T. von Kármán, *Aerodynamics* (McGraw-Hill, 1954).
 [4] O. Pironneau, "On optimum profiles in Stokes flow," *J. Fluid Mech.* **59**, 117 (1973).
 [5] B. Bourot, "Numerical computation of optimal profile in

- Stokes flow," *J. Fluid Mech.* **65**, 513 (1974).
- [6] O. Pironneau, "On optimum design in fluid mechanics," *J. Fluid Mech.* **64**, 97 (1974).
- [7] D. W. Kim and M.-U. Kim, "Minimum drag shape in two-dimensional viscous flow," *Int. J. Num. Meth. Fluids* **21**, 93 (1995).
- [8] B. Mohammadi and O. Pironneau, "Shape optimization in fluid mechanics," *Ann. Rev. Fluid Mech.* **36**, 11.1 (2004).
- [9] G. Batchelor, *Introduction to fluid dynamics* (C.U. Press, 1967).
- [10] I. Proudman and J. R. A. Pearson, "Expansions at small Reynolds numbers for the flow past a sphere and a circular cylinder," *J. Fluid Mech.* **2**, 237 (1957).
- [11] W. Chester, "On Oseen's approximation," *J. Fluid Mech.* **13**, 557 (1962).
- [12] H. Brenner and R. G. Cox, "The resistance to a particle of arbitrary shape in translational motion at small Reynolds numbers," *J. Fluid Mech.* **17**, 561 (1963).
- [13] J. Happel and H. Brenner, *Low Reynolds Number Hydrodynamics* (Martinus Nijhoff Publishers, 1973), 2nd ed.
- [14] S. Goldstein, "The forces on a solid body moving through a viscous fluid," *Proc. Roy. Soc. A* **123**, 216 (1929).
- [15] S. Kim and S. J. Karrila, *Microhydrodynamics: Principles and selected applications* (Butterworth-Heinemann, 1991).
- [16] W. Chester and D. R. Breach, "On the flow past a sphere at low Reynolds number," *J. Fluid Mech.* **37**, 751 (1969).
- [17] R. Cox, "The steady motion of a particle of arbitrary shape at small Reynolds numbers," *J. Fluid Mech.* **23**, 625 (1965).
- [18] G. Carrier, *Tech. Rep.*, ONR Mathematical Sciences Division (1953).